found by Phillies is proportional to $\nabla \cdot \mathbf{D}_{ik}$, which is zero for hydrodynamic interactions considered, as in this paper, at the Oseen level (eq 5.2).
(25) Yamakawa, H. "Modern Theory of Polymer Solutions"; Harper and Row: New York, 1971.
(26) Burchard, W.; Schmidt, M.; Stockmayer, W. H. *Macromolecules* **1980**, *13*, 580-7.
(27) Dubois-Violette, E.; de Gennes, P.-G. *Physics (Long Island City, N.Y.)* **1967**, *3*, 181-198.
(28) de Gennes, P.-G. *Physics (Long Island City, N.Y.)* **1967**, *3*, 37.
(29) Schurr, J. M., private communication (1980).
(30) Rarity, J. G., private communication.
(31) Nishio, I.; Swislow, G.; Sun, S.-T.; Tanaka, T. *Nature (London)* **1982**, *300*, 243-4.
(32) Schaefer, D. W.; Martin, J. E.; Wiltzius, P.; Cannell, D. S. *Phys. Rev. Lett.* **1984**, *52*, 2371-4.
(33) Martin, J. E.; Schaefer, D. W. *Phys. Rev. Lett.* **1984**, *53*, 2457-60.
(34) Weitz, D. A.; Huang, J. S.; Lin, M. Y.; Sung, J. *Phys. Rev. Lett.* **1984**, *53*, 1657-60.

Light Scattering Studies of Poly(methyl methacrylate)/[Poly(ethyl acrylate)/Poly(butyl acrylate)] Terpolymer

Benjamin Chu,*†‡ Qicong Ying,† Day-chyuan Lee,† and Dan-qing Wu†

Department of Chemistry and Department of Materials Science and Engineering, State University of New York at Stony Brook, Long Island, New York 11794-3400.
Received November 12, 1984

ABSTRACT: The classical Bushuk-Benoit light scattering theory for solutions of copolymers is extended to solutions of (quasi)terpolymers which may be polydisperse in chain composition as well as in molecular weight. A method for determining the weight-average molecular weight of a (quasi)terpolymer with only three solvents is described. The scheme was tested by using a poly(methyl methacrylate)/[poly(ethyl acrylate)/poly(butyl acrylate)] terpolymer (PMMA/[PEA/PBA]) and five solvents: methyl ethyl ketone (MEK), dioxane (DIO), ethyl acetate (EA), cyclohexanone (CYC), and *m*-dichlorobenzene (MDCB), covering a very broad refractive index increment range. The apparent molecular weight varies from 1.37×10^6 in ethyl acetate to 1.80×10^6 in cyclohexanone. One important factor in achieving a more precise molecular weight determination is the spread of the refractive index increment from -0.0391 in *m*-dichlorobenzene to 0.122 in ethyl acetate. The (true) molecular weight of the (quasi)terpolymer was determined to be $\sim 1.2 \times 10^6$. Intensity time correlation functions of PMMA/[PEA/PBA] in MEK, dioxane, and cyclohexanone were measured at different scattering angles as a function of concentration. By using a multiexponential singular value decomposition technique in the Laplace inversion and by taking into account the difference in the scattering power of the monomer-type components in different solvents, we were able to determine simultaneously the true molecular weight distribution and the chain composition of the polymer at different representative molecular weight fractions for the PMMA/[PEA/PBA] (quasi)terpolymer, provided that the properties of [PEA/PBA] are so similar as to have an average refractive index covering both monomer types.

I. Introduction

Light scattering has been used to determine the molecular weight of synthetic high polymers for nearly 40 years.[1] The application of this technique to copolymers has met with only limited success, partly because the molecular weight determination now requires at least three times the amount of work when compared with that for a homopolymer. The light scattering theory for copolymers[2] has also been extended to terpolymers where six solvents are recommended in order to resolve the same issue.[3] Consequently, absolute molecular weight determinations of copolymers and terpolymers by light scattering studies have remained a tedious method as few investigators are tempted to spend so much effort in order to just determine the molecular weight. Nevertheless, in present-day technology, we have increased usage in materials modification at the molecular level. Characterization of copolymers, terpolymers, or even more complex multicomponent polymers may be of interest.

The theoretical treatment for determining the molecular weights of copolymers was developed by Stockmayer et al.[4] and expressed in a more useful form by Bushuk and Benoit[2] almost 25 years ago. Since then, only a handful of experiments[5-10] with some emphasis on copolymer conformation have been reported. Although a straightforward extension of the Bushuk-Benoit theory to terpolymers has been worked out by Kambe et al.,[3] to our knowledge, no definitive experiments on light scattering molecular weight characterization of a terpolymer solution have ever been reported. In this article, we want to use the Bushuk-Benoit theory for the molecular weight determination of a (quasi)terpolymer in solution and to take advantage of recent developments in the Laplace inversion technique which permits us to measure characteristic line-width distributions from intensity time correlation functions. If we take into account the effect of scattering power by different monomer types of the "terpolymer" in different solvents, we have succeeded in determining simultaneously the molecular weight distribution and the "terpolymer" composition in different representative polymer molecular weight fractions. It should be noted that we have taken PEA/PBA as a single monomer type with PMMA being the other because the refractive index increments of PEA and PBA are very similar. Thus, the notation "(quasi)-terpolymer" is used and the method of analysis is essentially the same as that for a copolymer.

On the basis of the assumption of the additivity of refractive index increments of the components of a multicomponent polymer in a single solvent

$$\nu = (\mathrm{d}n/\mathrm{d}C)_{\text{polymer}} = \sum_{j=1} W_j \nu_j \qquad (1)$$

where ν_j [$\equiv (\mathrm{d}n/\mathrm{d}C)_j$] is the change of the refractive index n with respect to concentration C for monomer type j and

† Department of Chemistry.
‡ Department of Materials Science and Engineering.

0024-9297/85/2218-1962$01.50/0

W_j denotes the weight fraction of monomer type j in the polymer with $\sum_{j=1} W_j = 1$, we can determine the chain composition of the copolymer provided that refractive index increments of the monomer-type components in the copolymer differ markedly. Equation 1 is generally valid for block copolymers but may be difficult to justify for purely random copolymers. It should be noted that when the magnitude of the refractive index increments for one of the monomer types $(dn/dC)_A$ is very large, deviation from the additivity rule is no longer negligible; i.e., the interaction between A and solvent will now be affected by the interactions between A and B in the polymer chain or $(\partial V/\partial W_A)_{S,T,W_B=0} \neq (\partial V/\partial W_A)_{S,T,W_B}$, with V being the total volume and S and T indicating solvent and temperature.

Instead of different single solvents to cover large ranges of refractive index increment, determination of heterogeneous multicomponent polymers can be achieved with mixed solvents, which offer a variety of advantages.[11,12] The corresponding complications due mainly to preferential adsorption (or binding) can be resolved by making light scattering and refractive index increment measurements at constant chemical potential. Experimentally, we need to establish a dialysis equilibrium between the copolymer solution and the mixed solvent prior to our measurements if mixed solvents are used. Differential refractometry and light scattering on nylon-b and poly(methyl acrylate) in mixed solvents have been reported by Huglin and Richards.[13] In the present study, we have avoided the use of mixed solvents because we want to cover a very broad refractive index increment range, even though the use of mixed solvents would have been feasible.

II. Theoretical Treatment

1. Static Light Scattering. The excess Rayleigh ratio R_{vv} for vertically polarized incident and scattered light due to monodisperse homopolymers of molecular weight M and concentration C when extrapolated to infinite dilution and zero scattering angle has the form

$$\lim_{\substack{C\to 0\\ \theta\to 0}} (H^*C/R_{vv}) = 1/(M\nu^2) \tag{2}$$

where $H^* = 4\pi^2 n^2/(N_A\lambda_0^4)$, with n, N_A, and λ_0 being respectively the refractive index, the Avogadro number, and the incident wavelength in vacuo. For polydisperse homopolymers of uniform refractive index increment, we have

$$\lim_{\substack{C\to 0\\ \theta\to 0}} (H^*C/R_{vv}) = 1/(M_w\nu^2) \tag{3}$$

where $M_w = \sum_i W_i M_i$, with the subscript i referring to polymer species of chain length i. At finite scattering angles and concentration

$$\frac{HC}{R_{vv}(\theta)} \cong \frac{1}{M_w P(KR_g)} + 2A_2C \tag{4}$$

where $H = H^*\nu^2$ and $1/P(KR_g) \cong 1 + K^2\langle R_g^2\rangle_z/3$, with K and R_g being the magnitude of the momentum transfer vector and the radius of gyration, respectively. From the static light scattering equation (4), we can determine the weight-average molecular weight M_w, the mean square z-average radius of gyration $\langle R_g\rangle$, and the second virial coefficient A_2. In sufficiently dilute solutions and at small scattering angles, such that $A_2C \ll 1$ and $KR_g \ll 1$, we retrieve mainly the measured M_w as an absolute calibration for the molecular weight distribution.

For a solution of copolymers with polydisperse chain length and composition, the excess Rayleigh ratio extrapolated to zero scattering angle and concentration, R_{vv}^0, can be related to the molecular weight and the refractive index increment by the relation[2]

$$R_{vv}^0 = H^*\sum_i C_i M_i \nu_i^2 \tag{5}$$

Therefore, in a plot of $\lim_{K\to 0}(HC/R_{vv})$ vs. C, we get an intercept corresponding to M_{app}^{-1} with the apparent molecular weight

$$M_{app} = \frac{1}{\nu^2}\sum_i W_i M_i \nu_i^2 \tag{6}$$

where ν is the refractive index increment of the copolymer solution and $W_i = C_i/C$. However, for each molecular weight M_i, there can be a heterogeneity in composition such that ν_i ($\equiv\sum_j W_{ij}\nu_j$) is represented by the same j expression as in eq 1. Here we should recall that the subscripts i and j refer to chain length and monomer types, respectively. For example

$$\nu_i = W_{iA}\nu_A + W_{iB}\nu_B + W_{iC}\nu_C \tag{7}$$

for a copolymer with monomer types j = A, B, and C where ν_i is the refractive index increment for molecules with molecular weight M_i and weight fraction W_i whose composition is governed by eq 7. However, eq 7 is not unique because there can be a distribution of chain composition yielding the same M_i and W_i. Following the same reasoning, there can be polymers of different chain compositions and molecular weights having the same translational diffusion coefficient. Thus, our model refers to only the average chain[9] composition W_{ij} and the average refractive index increment ν_i having a molecular weight M_i and diffusion coefficient D_i^0. For each polymer species i, we have

$$W_{iA} + W_{iB} + W_{iC} = 1 \tag{8}$$

Similarly, for the whole copolymer, we have

$$W_A + W_B + W_C = 1 \tag{9}$$

by definition. If we let $\delta W_{iA} = W_{iA} - W_A$, $\delta W_{iB} = W_{iB} - W_B$, and $\delta W_{iC} = W_{iC} - W_C$, then

$$\delta W_{iA} + \delta W_{iB} + \delta W_{iC} = 0 \tag{10}$$

By substituting eq 7–10 into eq 6, we get

$$M_{app} = \sum_i W_i M_i \left[\frac{W_{iA}\nu_A + W_{iB}\nu_B + W_{iC}\nu_C}{\nu}\right]^2$$

which can be written as[3]

$$M_{app} = M_w + 2P_A\left(\frac{\nu_A - \nu_C}{\nu}\right) + 2P_B\left(\frac{\nu_B - \nu_C}{\nu}\right) + Q_A\left(\frac{\nu_A - \nu_C}{\nu}\right)^2 + Q_B\left(\frac{\nu_B - \nu_C}{\nu}\right)^2 + 2\left(\frac{\nu_A - \nu_C}{\nu}\right)\left(\frac{\nu_B - \nu_C}{\nu}\right) R_{AB} \tag{11}$$

with

$$P_A = \sum_i W_i M_i \delta W_{iA}$$

$$P_B = \sum_i W_i M_i \delta W_{iB}$$

$$Q_A = \sum_i W_i M_i (\delta W_{iA})^2$$

$$Q_B = \sum_i W_i M_i (\delta W_{iB})^2$$

$$R_{AB} = \sum_i W_i M_i (\delta W_{iA})(\delta W_{iB}) \tag{12}$$

According to eq 11, we would need a minimum of six solvents in order to determine the six unknowns: P_A, P_B,

Q_A, Q_B, R_{AB}, and M_w. Furthermore, such a determination would be difficult because of experimental error limits. However, in practice, if the difference in the refractve index increments of two of the monomer types in a terpolymer is relatively small when compared with the difference with respect to the third monomer type, e.g., $|\nu_{PMMA} - \nu_{PEA}|$ (or $|\nu_{PMMA} - \nu_{PBA}|$) $\gg |\nu_{PEA} - \nu_{PBA}|$ and if the changes in the difference of the refractive index increments between the monomer types in different solvents are relatively small, we can then simplify eq 11 to a more manageable form to be discussed in the Results and Discussion.

2. Dynamic Light Scattering. Precise measurements of the intensity time correlation function $[G^{(2)}(t)]$ in polymer solution at dilute concentrations by means of photon correlation spectroscopy and subsequent correlation function profile analysis permit an estimate of the polymer hydrodynamic size (R_h) distributions.[14-16] From the combined measurements of static and dynamic light scattering, we can determine the *absolute* molecular weight distribution (MWD) provided that we know the relation between the translational diffusion coefficient (D_T) and the molecular weight (M) for the specific polymer–solvent system and that the effects of interparticle interactions (A_2) and of the intramolecular interference $[P(KR_g)]$ are negligible.

The measured single-clipped photoelectron count autocorrelation function $G_k^{(2)}(t)$ is related to the normalized electric field autocorrelation function $g^{(1)}(t)$ by the relation

$$G_k^{(2)}(t) = A(1 + b|g^{(1)}(t)|^2) \tag{13}$$

where A is the background and b accounts for the nonideal point detector. The net intensity autocorrelation function, $G_k^{(2)}(t) - A = Ab|g^{(1)}(t)|^2$, is directly related to the measured unnormalized electric field autocorrelation function $(Ab)^{1/2}|g^{(1)}(t)|$. For independent identical polymer molecules undergoing only translational Brownian motions

$$|g^{(1)}(t)| = e^{-\Gamma t} \tag{14}$$

where $\Gamma = D_T K^2$, with D_T being the translational diffusion coefficient. In a dilute polydisperse polymer solution, each (structureless) particle of size i has a characteristic frequency Γ_i (due only to translational motions) and

$$|g^{(1)}(t)| = \sum_i a_i \exp(-\Gamma_i t) \tag{15}$$

where the weighting factor a_i is proportional to the time-average intensity scattered by species i at scattering vector K. In the limit of dilute concentrations and small K so that $P(KR_g) = 1$, $a_i \propto M_i^2$.

In a continuous line-width distribution, we have

$$|g^{(1)}(t)| = \int_0^\infty G(\Gamma) \exp(-\Gamma t)\, d\Gamma \tag{16}$$

where $G(\Gamma)$ is the normalized distribution of line widths. In practice, $g^{(1)}(t)$ contains noise and the integral in eq 16 has upper (b_0) and lower (a_0) bounds. Thus, the Laplace inversion is a very difficult ill-conditioned problem. Several methods, including the use of additional constraints and regularization, have been reported. In our case, we have found the singular value decomposition (SVD) for the solution of the linear problem arising from multiexponential approximations to be the most convenient.[17]

In the multiexponential approach, we approximate $G(\Gamma)$ as

$$G(\Gamma) = \sum_{q=1}^{Q} a_q \delta(\Gamma - \Gamma_q) \tag{17}$$

and

$$|g^{(1)}(\tau)| = \sum_{q=1}^{Q} a_q \exp(-\Gamma_q t) \tag{18}$$

where the subscript q denotes the qth representative monodisperse fraction of MWD based on the multiexponential model, not the qth individual polymer species as represented by eq 15. The number of basis functions used in the SVD analysis varies from 2 to 5, depending on the signal-to-noise ratio of $g^{(1)}(t)$ and the support ratio γ ($\equiv b_0/a_0$), although Q is expressed as many dependent δ functions, usually of the order of 20. The SVD analysis shown did not have any bins with negative amplitudes.

In a dilute polymer solution at finite concentration and scattering angle, we have to take into account both the interparticle interaction and the polymer intramolecular interference effects. The concentration effect can be represented by a second virial coefficient expansion

$$D_T = D_T^\circ(1 + k_d C) \tag{19}$$

where we have taken the measured second virial coefficient for diffusion (k_d) for the *overall* polymer–solvent system to be independent of molecular weight, an approximation that breaks down for very broad molecular weight distributions. However, for sufficiently dilute solutions, the correction for the diffusion coefficient from finite concentrations to infinite dilution merely represents a uniform shift of the diffusion coefficient distribution function along the x (diffusion coefficient) axis and accounts for no more than a few percent of the total concentration effect. Therefore, it is a relatively minor effect which we have taken into account.

At finite scattering angles, the characteristic line width contains information on internal motions of the polymer as well as its translational motions. $\Gamma = D_T K^2$ is no longer valid if $R_g K \gg 1$. We then have[18]

$$\Gamma \approx D_T K^2(1 + f\langle R_g^2\rangle K^2) \tag{20}$$

where f is a dimensionless number and depends on chain structure, polydispersity, and solvent quality. The coefficient f has been computed for a number of Gaussian models. For example, $f \sim 0.18$ without preaveraging the hydrodynamic interactions.

In plots of $G(K,\Gamma)$ vs. Γ at different scattering angles, the transformation to molecular weight distribution (e.g., weight fraction vs. molecular weight) can be achieved by considering a transform of $G(K,\Gamma)$ to representative weight fractions (W_q) along the y axis and of Γ_q to molecular weight (M_q) along the x axis. Our procedure for the transformation can best be represented by the schematic flow chart shown in Figure 1. The details will be discussed in the Results and Discussion. Suffice it to state here that the essential equations required for the transform are presented in this section.

In a *discrete* representative distribution of $G(K,\Gamma)$ vs. $\Gamma(K)$, the transform of Γ_q to molecular weight M_q along the x axis is relatively simple. By means of eq 20, if we plot $\Gamma_q(K)/K^2$ vs. K^2, we can determine for each q representative fraction the translational diffusion coefficient of the qth representative fraction at finite $D_q(C)$, where the subscript T has been omitted. The concentration dependence of D_q is then corrected by means of eq 19 in which we have taken k_d to be the *overall* second virial coefficient of the polymer–solvent system. This approximation is acceptable so long as the solution concentration is sufficiently dilute that $k_d C \ll 1$. At infinite dilution, we have

$$D_T^\circ = k_D M^{-\alpha_D} \tag{21}$$

where k_D is a proportionality constant and α_D is the exponent depending upon the solvent quality and chain

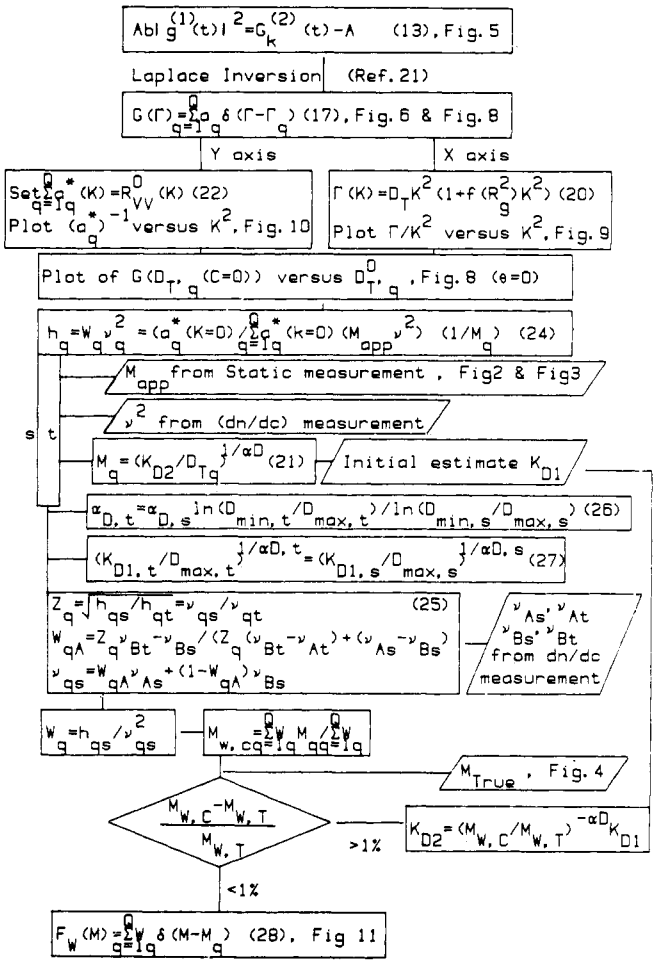

Figure 1. Procedure for determination of molecular weight distribution and monomer type composition for a copolymer using two solvents.

structure. In our analysis, we have assumed α_D in all reasonably good solvents, such as MEK, dioxane, and cyclohexanone, to be $\sim$0.56. Therefore, for a homopolymer solution, we can determine k_D once $D_T°$ and M are known. We have estimated the change in the magnitude of α_D on M_w/M_n and found small variations of $\alpha_D \sim 0.56 \pm 0.02$ to be acceptable uncertainties in the present context.[16] For a polydisperse homopolymer solution, the z-average translational diffusion coefficient at infinite dilution $D_z°$ from dynamic light scattering and the weight-average molecular weight M_w are often used to determine an average $\bar{k}_D$ based on the empirical expression $D_z° = \bar{k}_D M_w^{-\alpha_D}$. However, for a polydisperse copolymer solution, the averaging process, based on eq 5 and 17, is more complex because of possible composition changes in different molecular weight fractions. Nevertheless, for each representative molecular weight fraction M_q, we take the expression

$$D_{T,q}° = \bar{k}_D M_q^{-\alpha_D} \tag{21'}$$

to remain valid. In eq 21, $\bar{k}_D$ becomes an adjustable parameter for the copolymer–solvent system and is to be determined together with the monomer type composition for each representative molecular weight fraction (M_q).

Along the y axis, in transforming $G(\Gamma_q)$ [$\equiv a_q(K)$] to W_q, we first set

$$\sum_{q=1}^{Q} a_q(K) = R_{vv}°(K) \tag{22}$$

and then plot $a_q^{*-1}(K)$ vs. K^2 at fixed values of q. The asterisk indicates a renormalization of the intensity amplitude factors a_q for the representative fractions. By extrapolation to zero scattering angle and after correction for the concentration effect, we have

$$a_q^*(K = 0) = H^* C_q M_q \nu_q^2 \tag{23}$$

for each representative fraction q. By combining eq 22, 23, and 5, we can determine a composite amplitude factor h_q

$$h_q = W_q \nu_q^2 = [a_q^*(K = 0)/R_{vv}°](M_{app}\nu^2)/M_q \tag{24}$$

where $a_q^{*-1}(K = 0)$ is the intercept in the a_q^{*-1} vs. K^2 plot. $R_{vv}°$ and M_{app} are from static light scattering experiments, ν ($\equiv dn/dc$ of the copolymer in a given solvent) is determined experimentally with a differential refractometer, and $M_q \propto D_{T,q}^{\circ -1/\alpha_D}$ with $\bar{k}_D$ being an adjustable parameter according to eq 21'. The composite amplitude h_q ($\equiv W_q \nu_q^2$) contains information on the weight fraction W_q of the qth representative fraction having molecular weight M_q and the change of the refractive index n with respect to concentration C for monomer types PMMA and PEA/PBA having a total molecular weight M_q. According to eq 7, we have

$$\nu_q = W_{qA}\nu_A + W_{qB}\nu_B \tag{7'}$$

where the subscripts A and B represent PMMA and PEA/PBA. In eq 7', we have assumed PEA/PBA to be one monomer type because the refractive index increments for PEA and PBA in different solvents are nearly the same. This approximation introduces only a small error and its effects will be discussed later. In order to separate the effects of W_q and ν_q in eq 24, we need to repeat the above analysis in two different solvents (s and t) since W_q is independent of solvents while ν_q is a function of solvent refractive index. Thus, by comparing the composite amplitude factor in two different solvents, we get

$$Z_q = (h_{q,s}/h_{q,t})^{1/2} = \nu_{q,s}/\nu_{q,t} \tag{25}$$

whereby we can solve for W_{qA} and W_{qB} (=1 – W_{qA}) provided that $\nu_{A,s}$, $\nu_{B,s}$, $\nu_{A,t}$, and $\nu_{B,t}$ are known. The ν values for the monomer types can again be determined independently by using a differential refractometer. With known ν_q, we can then compute W_q. Thus, we have a plot for the molecular weight distribution (MWD) based on representative fractions W_q vs. M_q. From MWD, we can compute $\sum_{q=1}^{Q} W_q M_q = M_w$, which can be compared with the (true) molecular weight as determined by static light scattering. It should be noted that in our scheme, we have used $\bar{k}_D$ for the copolymer in one solvent as an adjustable parameter and that we need to know the value of α_D for one of the solvents. By taking advantage of the invariance in the representative molecular weight fractions, we can express the values of α_D in two different solvents as, according to eq 21'

$$\alpha_{D,t} = \alpha_{D,s}[\ln (D_{min,t}/D_{max,t})]/[\ln (D_{min,s}/D_{max,s})] \tag{26}$$

where the subscripts min and max denote the lowest and the highest representative fractions originating from a discrete $G(\Gamma)$ vs. Γ plot. Thus, we can determine the ratio of k_D in two different solvents by the relation

$$\left(\frac{k_{D,t}}{D_{max,t}}\right)^{1/\alpha_{D,t}} = \left(\frac{k_{D,s}}{D_{max,s}}\right)^{1/\alpha_{D,s}} \tag{27}$$

where we have used D_{max} as our more reliable reference purely based on experimental conditions. It should be emphasized that k_D is determined experimentally by combining $G(\Gamma)$ with M_w from static light scattering measurements; i.e., M_w permits us to slide the character-

Table I
Physical Properties of Solvents and Homopolymers

	polymer		
	PMMA	PEA	PBA
n^{30}_{488}[a]	1.4976	1.4741	1.4687
density (l), g/cm^3	1.188	1.12	1.087

	solvent				
	CYC	MDCB	DIO	EA	MEK
n^{30}_{488}[b]	1.4542	1.5427	1.4235	1.3725	1.3793
$\bar{v}_{PMMA}$,[c] cm^3/g	0.823[d]	0.8187[e]	0.8181	0.7963	0.7993

[a] n_{488} values for PMMA were interpolated from values of n_{589}, n_{546}, and n_{436} based on: Brandrup, J., Immergut, E. H., Eds. "Polymer Handbook"; Wiley: New York, 1975. n_{488} values for PEA and PBA were obtained from n_D values whereby we assumed the same correction factor for the wavelength dispersion as that of PMMA. [b] Measured with an Abbe refractometer after temperature and wavelength corrections. [c] "Polymer Handbook", at 25 °C except for $\bar{v}_{PMMA}$ in cyclohexanone. [d] $\bar{v}_{PMMA}$ measured by means of a density meter at 30 °C. [e] *o*-Dichlorobenzene instead of *m*-dichlorobenzene (MDCB).

istic line-width distribution function $G(\Gamma)$ along the molecular weight axis so that we can force the calculated (true) weight-average molecular weight to equal the measured (true) weight-average molecular weight. The final molecular weight distribution $F_w(M)$ has the form

$$F_w(M) = \sum_{q=1}^{Q} W_q \delta(M - M_q) \tag{28}$$

Similarly, we have

$$M_n = \sum_{q=1}^{Q} W_q / \sum_{q=1}^{Q} (W_q/M_q) \tag{29}$$

$$M_z = \sum_{q=1}^{Q} W_q M_q^2 / \sum_{q=1}^{Q} W_q M_q \tag{30}$$

and the associated cumulative distribution function $F_w(M)$, defined by

$$F_w(M) = \int_0^M F_w(M)\, dM / \int_0^\infty F_w(M)\, dM$$

III. Experimental Methods

1. Materials. The terpolymer Acryloid K-125 (lot no. 3-6326) is an all-acrylic polymer designed for general use as a processing aid in PVC compounds and is available in commercial quantities from Rohm and Haas Co., Philadelphia, PA. It has the appearance of a fine white free-flowing powder with a bulk density of 0.30 g/cm^3 and a specific gravity of 1.18. ^{13}C NMR analysis of the terpolymer in a pyridine–deuterated benzene mixture showed an estimated monomer ratio, by mole fraction, of 0.82 methyl methacrylate (MMA):0.12 ethyl acrylate (EA):0.06 butyl acrylate (BA),[19] with uncertainties of about 3%. Some physical properties of the solvents (refractive index at 488 nm and 30 °C (n^{30}_{488}) and partial specific volume of PMMA ($\bar{v}_{PMMA}$)) and of the monomer types (PMMA, PEA, and PBA) are listed in Table I.

Refractometry. Specific refractive index increments were measured with a Brice Phoenix differential refractometer fitted with an external circulator thermostat controlled to ±0.02 °C. Values of ν ($\equiv(\partial n/\partial C)_{T,P}$) for the various monomer types and the terpolymer in different solvents were determined at 30 °C and λ_0 = 436 and 546 nm. The interpolated values at 488 nm and 30 °C are listed in Tables II and III.

2. Light Scattering. Most stock solutions were prepared at ~10^{-3} g/cm^3. For each concentration, known weights of the stock solution and of the solvent were filtered directly into the light scattering cell using Teflon (Millipore FG) filters of 0.2-μm pore diameter. Light scattering intensity measurements were made at λ_0 = 488 nm and 30 °C with a light scattering spectrometer which has been described elsewhere.[15]

IV. Results and Discussion

1. Refractive Index Increments. Equation 11 can be simplified if $\nu_A - \nu_C$ and $\nu_B - \nu_C$ are relatively constant in different solvents. For the PMMA/[PBA/PEA] terpolymer, we can demonstrate that the term ($\nu_{PMMA} - \nu_{PBA}$) is relatively constant in different solvents and the term ($\nu_{PEA} - \nu_{PBA}$) is very small when compared with ($\nu_{PMMA} - \nu_{PBA}$). Therefore, even if the value of ($\nu_{PEA} - \nu_{PBA}$) is different in different solvents, the simplified form (eq 32) for molecular weight determination remains valid. In order to estimate the refractive index increments of the homopolymer, we used the Lorenz–Lorentz equation[20]

$$\nu_j = \frac{(n_{solv}^2 + 2)^2}{6n_{solv}} \left[v_j \left(\frac{n_j^2 - 1}{n_j^2 + 2} \right) - \bar{v}_j \left(\frac{n_{solv}^2 - 1}{n_{solv}^2 + 2} \right) \right] \tag{31}$$

The calculated values for ν_j are listed in Table II. We have also measured ν_j for selected homopolymer–solvent systems. The measured and calculated (based on eq 31) values of ν_j are in reasonable agreement. Values of ν_{measd} for PEA and PBA are somewhat less reliable because the PEA and PBA samples were available commercially only in toluene solution. It was difficult to remove all traces of toluene. As values of n_{PBA}, n_{PEA}, and n_{CYC} are close to one another, the measured values of ν_{PEA} and ν_{PBA} in CYC become less reliable. According to values listed in Table II, ($\nu_{PMMA} - \nu_{PBA}$) varies from 0.031 to 0.036 while ($\nu_{PEA} - \nu_{PBA}$) varies from 0.003 to 0.005. Thus, ($\nu_A - \nu_C$) is relatively constant (to within ~10%) even when we vary the solvent refractive index from 1.37 to 1.54. Although variations of ($\nu_B - \nu_C$) may approach ~40%, the effect becomes negligible because its magnitude is relatively small. For example, $\nu_{terpolym}$ in MEK and CYC is 0.1081 and 0.0396, respectively, while ($\nu_{PMMA} - \nu_{PBA}$) = 0.033 and 0.031 and ($\nu_{PEA} - \nu_{PBA}$) = 0.0034 and 0.0043 in the same two solvents, respectively. Thus, we can write

$$M_{app} = M_w + (1/\nu)[2P_A(\nu_a - \nu_C) + 2P_B(\nu_B - \nu_C)] + (1/\nu^2)[Q_A(\nu_A - \nu_C)^2 + Q_B(\nu_B - \nu_C)^2 + 2R_{AB}(\nu_A - \nu_C)(\nu_B - \nu_C)]$$

or

$$M_{app} \approx M_w + P^*/\nu + Q^*/\nu^2 \tag{32}$$

Table II
Refractive Index Increments of Homopolymers at 30 °C and 488 nm[a]

	ν_{PMMA}		ν_{PEA}		ν_{PBA}		$\nu_{PEA/PBA}$[b]			
solvent	calcd	measd	calcd	measd	calcd	measd	calcd	measd	$(\nu_{PMMA} - \nu_{PBA})_{calcd}$	$(\nu_{PEA} - \nu_{PBA})_{calcd} \times 10^3$
DIO	0.0726	0.0720	0.0449	0.0446	0.0415	0.0434	0.0438	0.0442	0.0319	3.4
CYC	0.0471	0.0456	0.0195	0.017	0.0152	0.021	0.0181	0.018	0.0311	4.3
MEK	0.1140		0.0843	0.0880	0.0809	0.0879	0.0832	0.0880	0.0331	3.4
EA	0.1197		0.908		0.0858		0.0891		0.0339	5.0
MDCB	−0.0314		−0.0630		−0.0678		−0.0646		0.0364	4.8

[a] Calcd and measd denote calculated and measured values, respectively. ν_{calcd} was based on eq 31 and values of $v_{polym}(1/\rho_{polym})$, $\bar{v}_{polym}$, n_{polym}, and n_{solv}. For PEA and PBA, we assumed $\bar{v} = v$. [b] $\nu_{PEA/PBA} \simeq {}^2/_3\nu_{PEA} + {}^1/_3\nu_{PBA}$ based on ^{13}C NMR analysis.[19]

Table III
Molecular Parameters of Terpolymer PMMA/[PEA/PBA]

parameter	solvent				
	MEK	DIO	EA	CYC	MDCB
ν_{calcd}	0.1085	0.0674	0.1142	0.419	−0.0374
$\nu_{measd}(488)$	0.1081	0.0674	0.1215	0.0396	−0.0391
% diff	0.2	0	3	3	2
$10^{-6}M_{app}$	1.53	1.59	1.37	1.80	1.70
$\langle R_{g,a}^2\rangle^{1/2}$, nm	73.6	78.3	80.8		115
10^4A_2, cm^3 mol/g^2	1.76	1.96	1.96		−0.75
k_d, cm^3 g	192.25	−2.91		431.99	

[a] Equation 1 with $W_{PMMA}:W_{PEA}:W_{PBA}$ = 82:12:6 and values of ν_{calcd} as listed in Table II.

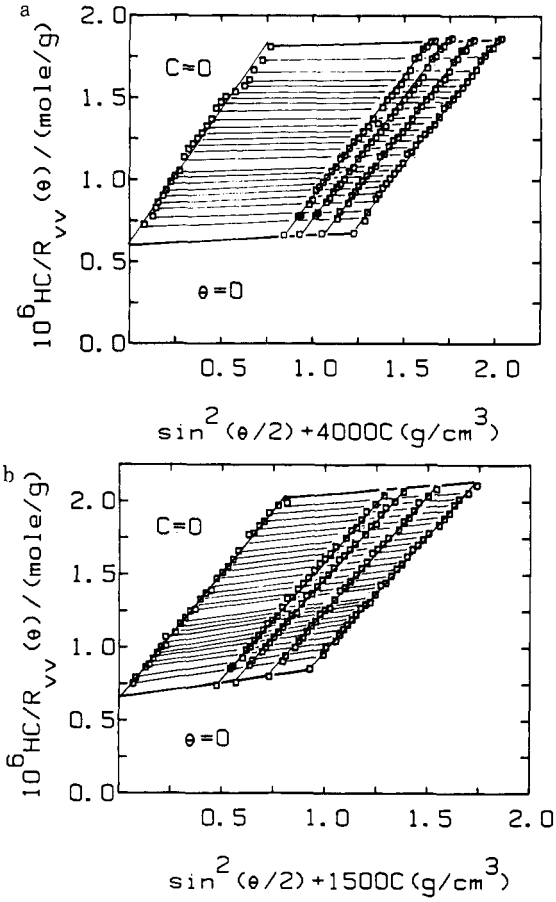

Figure 2. (a) Zimm plot of terpolymer (3-6326) in methyl ethyl ketone (MEK) at 30 °C. $C_1 = 3.049 \times 10^{-4}$ g/cm^3, $C_2 = 2.674 \times 10^{-4}$ g/cm^3, $C_3 = 2.374 \times 10^{-4}$ g/cm^3, and $C_4 = 2.138 \times 10^{-4}$ g/cm^3. (b) Zimm plot of terpolymer (3-6326) in dioxane (DIO) at 30 °C. $C_1 = 6.169 \times 10^{-4}$ g/cm^3, $C_2 = 4.855 \times 10^{-4}$ g/cm^3, $C_3 = 3.780 \times 10^{-4}$ g/cm^3, and $C_4 = 3.150 \times 10^{-4}$ g/cm^3.

where we have taken the values inside the brackets to be relatively constant, independent of different solvents with $P^* = 2P_A(\nu_A - \nu_C) + 2P_B(\nu_B - \nu_C)$ and $Q^* = Q_A(\nu_A - \nu_C)^2 + Q_B(\nu_B - \nu_C)^2 + 2R_{AB}(\nu_A - \nu_C)(\nu_B - \nu_C)$. The important point to be recognized here is that terpolymers can be approximated as copolymers provided that we are aware of the ν_j variations in different solvents.

In fact, we can try to take into account the variations in ν_j by writing eq 32 as a copolymer system

$$M_{app} \simeq M_w + \frac{2P(\nu_{PMMA} - \nu_{PEA/PBA})}{\nu} + Q\frac{(\nu_{PMMA} - \nu_{PEA/PBA})^2}{\nu^2} \quad (33)$$

Unfortunately, we do not yet have sufficient data to make a proper comparison between eq 32 and 33.

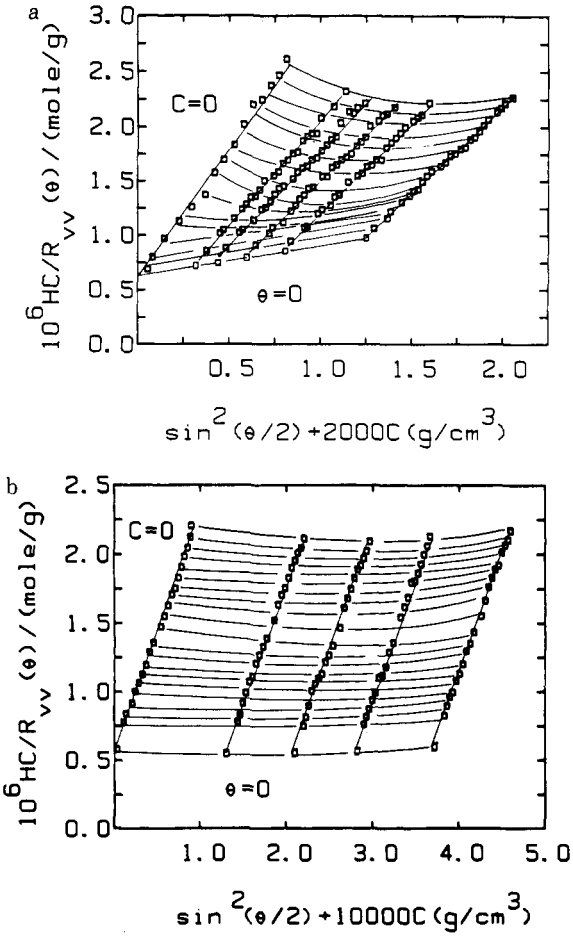

Figure 3. (a) Zimm plot of terpolymer (3-6326) in ethyl acetate (EA) at 30 °C. $C_1 = 6.20 \times 10^{-4}$ g/cm^3, $C_2 = 3.912 \times 10^{-4}$ g/cm^3, $C_3 = 2.953 \times 10^{-4}$ g/cm^3, $C_4 = 2.146 \times 10^{-4}$ g/cm^3, and $C_5 = 1.616 \times 10^{-4}$ g/cm^3. (b) Zimm plot of terpolymer (3-6326) in *m*-dichlorobenzene (MDCB) at 30 °C. $C_1 = 3.746 \times 10^{-4}$ g/cm^3, $C_2 = 2.800 \times 10^{-4}$ g/cm^3, $C_3 = 2.093 \times 10^{-4}$ g/cm^3, and $C_4 = 1.324 \times 10^{-4}$ g/cm^3.

2. Light Scattering Intensity Measurements. According to eq 4 and 6, the angular distribution of absolute scattered intensity for a copolymer in dilute solution has the form

$$\frac{HC}{R_{vv}} = \frac{1}{M_{app}}\left(1 + \frac{16\pi^2}{3\lambda^2}\langle R_{g,a}^2\rangle \sin^2(\theta/2)\right) + 2A_2C \quad (34)$$

where we have stressed the fact that light scattering intensity measurements in a dilute copolymer solution can determine only the apparent molecular weight and the apparent radius of gyration. Figures 2 and 3 show Zimm plots of the terpolymer in MEK, DIO, EA, and MDCB at 30 °C. While Figure 2 shows typical Zimm plots as encountered in solutions of homopolymers (although we get only M_{app} and $R_{g,a}$), Figure 3 represents the light scattering behavior for copolymers where we can more easily visualize that only apparent values could be determined. The results for the molecular parameters of the terpolymer are listed in Table III. The apparent radius of gyration can best be realized by examining its value in MDCB with $\langle R_{g,a}^2\rangle^{1/2} = 115$ nm and $A_2 = -0.75 \times 10^{-4}$ cm^3 mol/g^2 while $\langle R_{g,a}^2\rangle^{1/2} \sim 76$ nm with a positive A_2 ($\sim 1.9 \times 10^{-4}$ cm^3 mol/g^2) in MEK and DIO. By means of eq 32 and the values listed in Table III, we can determine the (true) weight-average molecular weight of the terpolymer (M_w) to be 1.2×10^6 as shown in Figure 4.

3. Dynamic Light Scattering Measurements. From photon correlation measurements, the net intensity time

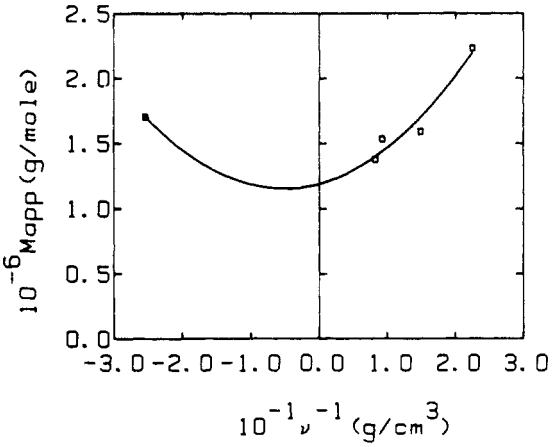

Figure 4. Plot of M_{app} vs. ν^{-1}. We have $M_{app} = 1.2 \times 10^6 + 1.4 \times 10^4\nu^{-1} + 1.36 \times 10^3\nu^{-2}$, with ν^{-1} expressed in g/cm^3. From left to right, the hollow squares denote MDCB, EA, MEK, DIO, and CYC, respectively.

correlation function $Ab|g^{(1)}(\tau)|^2$ of the terpolymer in solution exhibits non-single-exponential decay behavior, as shown in Figure 5. The refractive index increment variation influences the ratio of a_q in eq 17, which in turn yields apparent amplitudes for $g^{(1)}(\tau)$ in eq 18. By following the flow chart in Figure 1, we perform a Laplace inversion using the multiexponential approximation (eq 17 and 18) and the singular value decomposition technique. Figure 6 shows a typical analysis of $|g^{(1)}(\tau)|^2$ using $Q = 20$ in eq 17. However, a small number (k) of basis functions were used in order to avoid the ill-conditioning problem. The choice of k (= 2, 3, and 4) can be made on the basis of the behavior of the candidate solution vectors whose norm is defined by $||p^{(k)}|| = (\sum_{q=1}^{Q} a_q^2)^{1/2}$ and the resulting residual vectors $||r^{(k)}||$, with $||r^{(k)}|| = [\sum_{i=1}^{P}(|g^{(1)}(\tau_i)_{measd}| - |g^{(1)}(\tau_i)_{calcd}|)^2]^{1/2}$ and p being the number of data points in the correlation function. Acceptable solutions will have a small solution vector norm as well as a small residual norm. As illustrated in Figure 6, the most appropriate candidate solution corresponds to $k = 3$ or 4. In the Laplace inversion, we also take into account the fact that, for a unimodal size distribution function, which is implicitly assumed for the terpolymer, there are realistic upper and lower bounds for $G(\Gamma)$ and we should consider only the lowest candidate solution ($k = 3$ in the present case) which satisfies our criteria. Figure 7 shows plots of $Ab|g^{(1)}(\tau)|^2$ vs. delay channel number using the fitting results of Figure 6. From the percent deviation plot, we can see that the $k = 3$ and 4 candidate solutions fit the experimental data almost equally well. However, for the reasons already stated, i.e., we want to choose the lowest k value and prefer to have reasonable upper and lower bounds for $G(\Gamma)$, we have the $k = 3$ candidate solution as our $G(\Gamma)$. Figure 8 shows typical plots of $G(D^*)$ vs. D^* for the terpolymer in dioxane (a), cyclohexanone (b) and MEK (c) at a fixed finite concentration, $\theta = 45°$, 60°, and 90°, and 30 °C. The discrete representative fractions (q) have been scaled according to $\Gamma_q = D_q^* K^2$ along the x axis and $\sum_{q=1}^{Q} a_q^*(K) = R_{vv}(K)$ along the y axis. At finite scattering angles and for the larger molecular weight fractions, measurements of the characteristic line width include internal motions as expressed in eq 20. Thus, we need to plot Γ_q/K^2 vs. K^2, as shown typically in Figure 9, in order to obtain $D_{T,q}$ ($=\lim_{K\to 0}(\Gamma_q/K^2)$) at the intercept. By means of eq 19, we finally obtain $D_{T,q}°$ ($\lim_{C\to 0}^{K\to 0}(\Gamma_q/K^2) = \lim_{C\to 0} D_{T,q}$) as the translational diffusion coefficient for the qth representative fraction at infinite dilution. Along the y axis, we also need to correct for the intermolecular interference

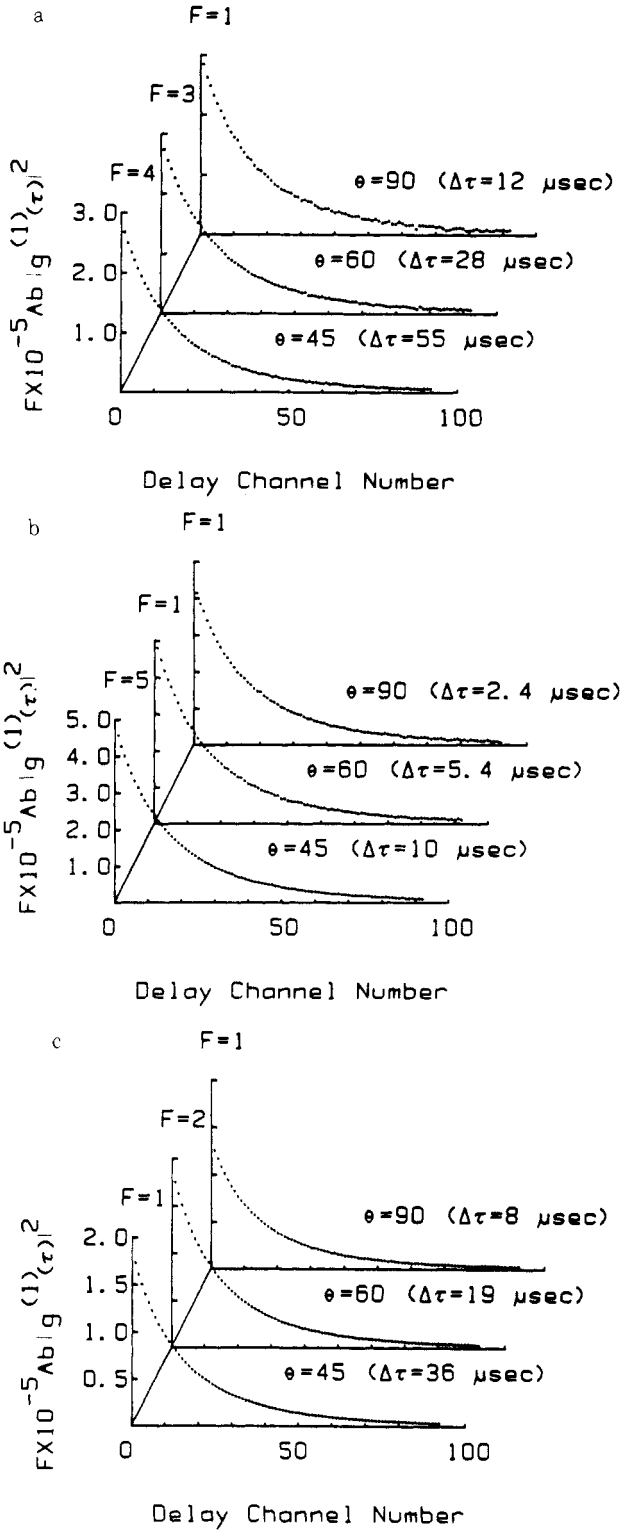

Figure 5. Typical measured net time correlation functions of terpolymer at 30 °C in various solvents, concentrations, and scattering angles: (a) dioxane, $C = 9.65 \times 10^{-4}$ g/mL; (b) cyclohexanone, $C = 4.46 \times 10^{-4}$; (c) MEK, $C = 9.29 \times 10^{-4}$. $\Delta\tau$ denotes the delay time increment and F is an arbitrary scaling factor.

term. Plots of $G^{-1}(D_q^*)$ ($\equiv a_q^{*-1}$) vs. K^2 yield straight lines, as shown typically in Figure 10 with $\lim_{K\to 0} a_q^* = H^* C_q M_q \nu_q^2$ for each representative qth fraction. The final composite plot of $H^* C_q M_q \nu_q^2$ ($\equiv\lim_{K\to 0} a_q^*$) vs. $D_{T,q}°$ is shown in Figure 8 by solid lines ($\theta = 0$). We should note that all our line-width distributions are discrete. The solid lines for $\theta = 0$ as shown in Figure 8 are curves that have been drawn by connecting the discrete δ functions which are represented by the vertical solid lines. According to

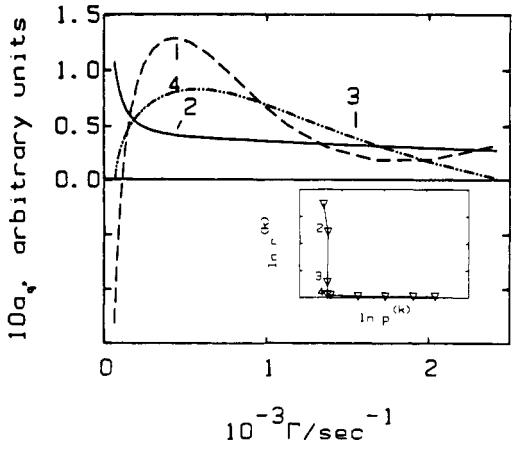

Figure 6. Plots of a discrete line width distribution in a_q vs. Γ based on candidate solutions in $P^{(k)}$ with $k = 2$, 3, and 4 for the terpolymer in dioxane at 30 °C, $\theta = 45°$, and $C = 9.65 \times 10^{-4}$ g/mL. The $k = 3$ solution is postulated as the optimal solution. Curves are drawn by connecting the discrete δ functions.

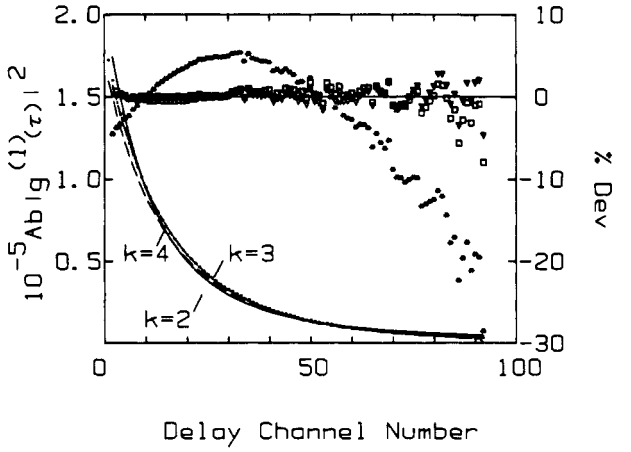

Figure 7. Plots of $Ab|g^{(1)}(\tau)|^2$ vs. delay channel number based on the results of Figure 6. % dev = $100(Ab|g^{(1)}(\tau)|_{measd}^2 - Ab|g^{(1)}(\tau)|_{calcd}^2)/Ab|g^{(1)}|_{measd}^2$. $k = 2$ (*), 3 (□), and 4 (▽). The dots are experimental data.

eq 23 and 24, we have determined the composite term $W_q\nu_q^2$ as a function of $D_{T,q}°$.

Following the procedure outlined in Figure 1 and using k_D for one of the solvents as an adjustable parameter, we finally obtain the molecular weight distribution of the terpolymer as shown in Figure 11 and composition of monomer types (PMMA and PEA/PBA) in each representative fraction q as shown in Figure 12. An alternative plot for Figure 11 is presented in Figure 13. In Figure 13, the cumulative weight fractions clearly show that the terpolymer has 95 wt % in the molecular weight range 3×10^5 to 3×10^6. In the composition curve (Figure 12) over the same molecular weight range, we see that the PMMA composition increases with increasing molecular weight. This conclusion was confirmed by using ^{13}C NMR measurements of different molecular weight fractions. Methanol was used to fractionally precipitate the terpolymer dissolved in MEK. Figure 14 shows ^{13}C NMR spectra of the high molecular weight fraction of the terpolymer, the unfractionated terpolymer, and the low molecular weight fraction of the terpolymer in deuterated chloroform. The trend clearly supports our conclusion.

In our extrapolation procedure, we have used eq 20 as shown in Figure 9 where slope/intercept = $f\langle R_{g,a}^2\rangle_q$ at a fixed concentration. The internal motion contributions to the characteristic line width can be scaled independently

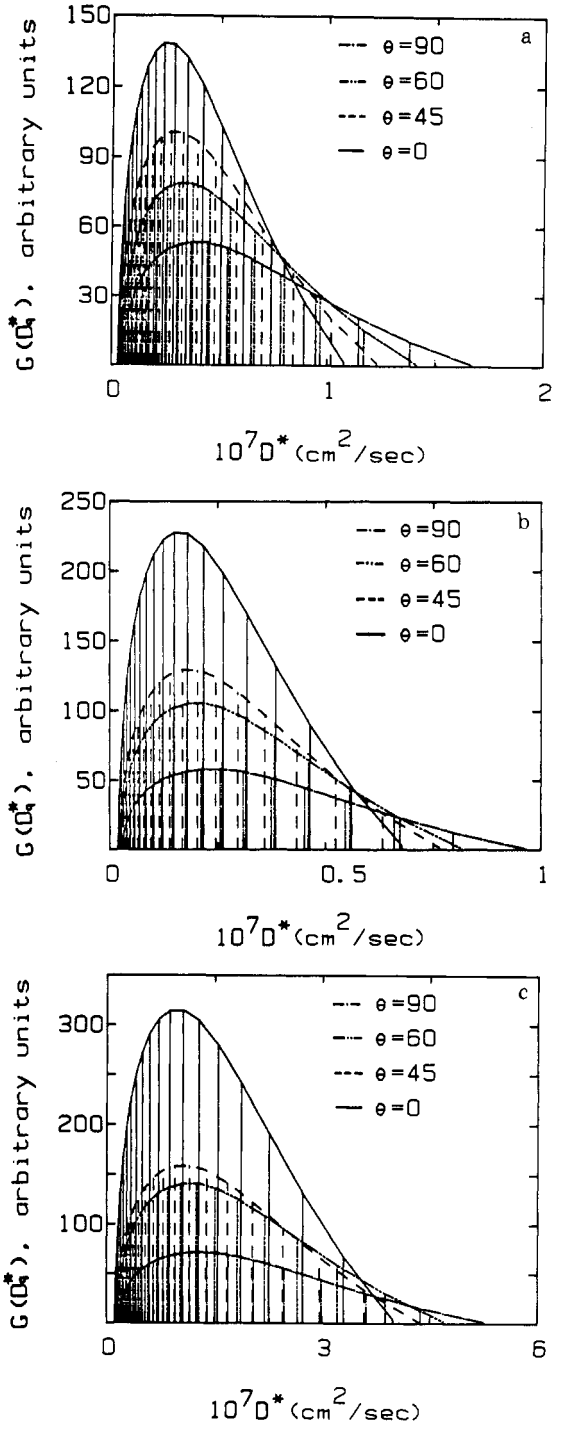

Figure 8. Plots of $G(D^*)$ vs. D^* for the terpolymer dissolved in different solvents at various scattering angles and fixed concentrations: (a) dioxane, $C = 9.65 \times 10^{-4}$ g/mL; (b) cyclohexanone, $C = 4.46 \times 10^{-4}$; (c) MEK, $C = 9.29 \times 10^{-4}$. At $\theta = 45°$, 60°, and 90°, we have set $\Gamma_q = D_q^*K^2$ and $\sum_{q=1}^{Q} a_q^*(K) = R_{vv}(K)[\lim_{K\to 0}(q/K^2) = D_{T,q}$. In addition, at $K = 0$, we have corrected for the concentration effect according to eq 19 with $D_{T,q}(K = 0, C = 0) = D_{T,q}(K = 0,C)/(1 + k_dC)$. The 20 representative fractions are labeled from 1 to 20 according to increasing D_q^* values.

by plotting $\bar{\Gamma}/K^2$ vs. K^2, with $\bar{\Gamma}$ [$\equiv \int_0^\infty G(\Gamma)\Gamma\, d\Gamma$] being an average characteristic line width, usually determined by the method of cumulants.[21] Figure 15 shows scaling of the three normalized time correlation functions at $\theta = 45°$, 60°, and 90° using the measured $f\langle R_{g,a}^2\rangle$ [$\equiv 8.10 \times 10^{-12}$ cm^2] value. It is interesting to note that the measured value of $f = 0.13$ is not far from the theoretical predictions.[18]

An interesting observation on why we are able to resolve the composition of the monomer types together with the

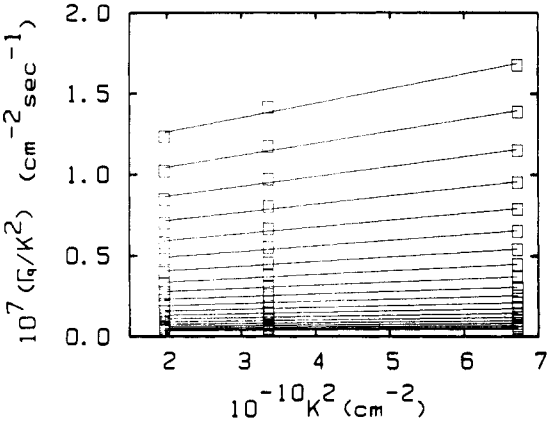

Figure 9. Plot of Γ_q/K^2 vs. K^2 for different representative fractions of terpolymer in dioxane at $C = 9.65 \times 10^{-4}$ g/mL. The 20 representative fractions from 1 to 20 are presented from bottom to top. Slopes are arbitrary. We considered only $\lim_{K\to 0} \Gamma_q/K^2$.

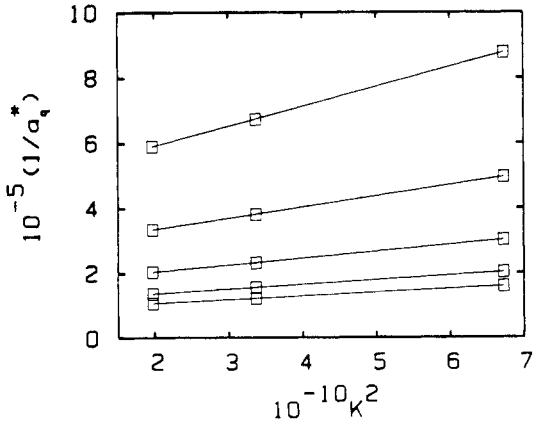

Figure 10. Plots of a_q^{*-1} vs. K^2 for some typical representative fractions of terpolymer in dioxane at $C = 9.65 \times 10^{-4}$ g/mL. The fraction number from bottom to top corresponds to 15, 13, 11, 9, and 7, respectively. We considered only $\lim_{K\to 0} a_q^*$.

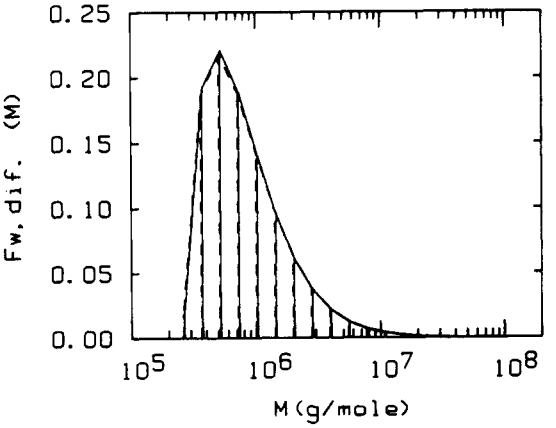

Figure 11. Molecular weight distribution of terpolymer (3-6326) using two solvent pairs. Solid line denotes CYC and DIO solvent pair. Dashed line denotes CYC–MEK solvent pair. $M_w/M_n \sim 1.8$ with $M_w = 1.2 \times 10^6$.

weight fraction of each representative q fraction can be illustrated by Figure 16, which shows plots of $W_q\nu_q^2$ vs. M_q for the results involving two solvent pairs: DIO–CYC and MEK–CYC. For each representative fraction, the molecular weight M_q and the weight fraction W_q are invariant. The different height is due to composition differences which can be solved by using two solvents of different refractive index provided that eq 1 is valid.

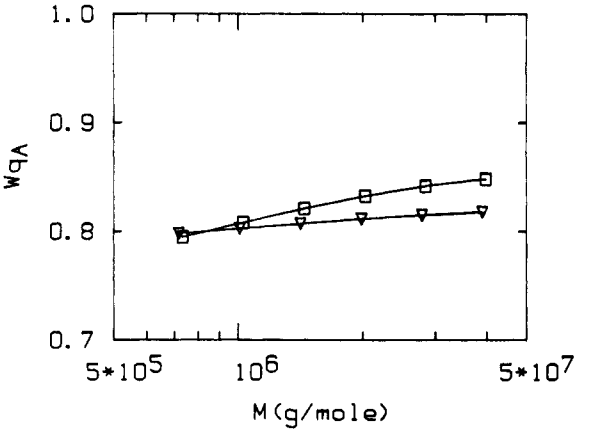

Figure 12. Composition of monomer types, PMMA and PEA/PBA, in each representative fraction q. Hollow squares denote W_{qA} using CYC–DIO solvent pair, with subscript A denoting PMMA. Hollow inverted triangles denote W_{qA} using CYC–MEK solvent pair. In comparing the shape of the two composition curves, we have scaled $W_A = 0.79$. In practice, $W_A = 0.78$, 0.83, and 0.77 in CYC, DIO, and MEK, respectively.

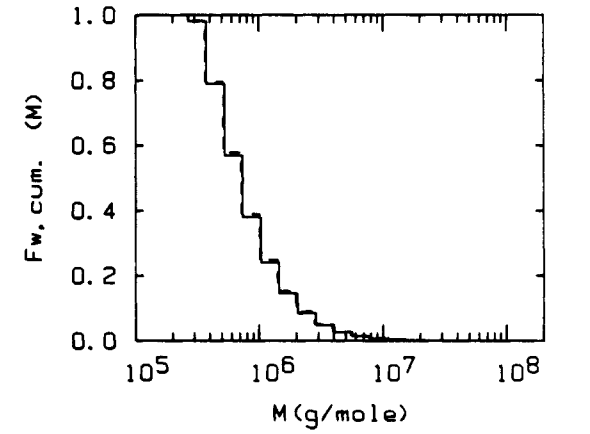

Figure 13. Cumulative molecular weight distribution of terpolymer based on Figure 11.

V. Conclusion and Further Remarks

The essential features of our scheme can best be summarized by the empirical eq 21, i.e., $D_T° = k_D M^{-\alpha_D}$. It implies that for a monodisperse copolymer there is a relationship between the translational diffusion coefficient and the molecular weight. Information on the refractive index increment of the copolymer, ν_{polym}, is not needed because both k_D and α_D are not related to ν_{polym}. On the other hand, a knowledge of the solvent is essential because we have assumed both k_D and α_D to be relatively independent of chain compositions. For example, this assumption breaks down if the solvent is a good solvent for monomer type A but a Θ solvent for monomer type B.

For PMMA in acetone at 20 °C, $D_z° = (8.09 \pm 0.68) \times 10^{-4} M_w^{-0.57\pm0.01}$ and in butyl chloride at 34.5 °C, $D_z° = (3.08 \pm 0.68) \times 10^{-4} M_w^{-0.50\pm0.01}$, with $D_z°$ and M_w expressed in cm^2/s and g/mol, respectively.[22] In our case, we determined $D_z° = 3.02 \times 10^{-4} M_w^{-0.56}$ for PMMA in methyl methacrylate (MMA).[16] We obtained $D_z° = 3.8 \times 10^{-4} M_w^{-0.56}$ for the PMMA/[PEA/PBA] terpolymer in methyl ethyl ketone at 30 °C using the assumption that $\alpha_D \sim 0.56$. A numerical value of $k_D \sim 3.8 \times 10^{-4}$ is comparable to those of PMMA. Furthermore, if we were to change α_D by ±0.02, the polydispersity index (M_w/M_n) would change by less than 3% of 1.8.

For a polydisperse copolymer with varying chain composition, we have eq 6 for M_{app} from static light scattering

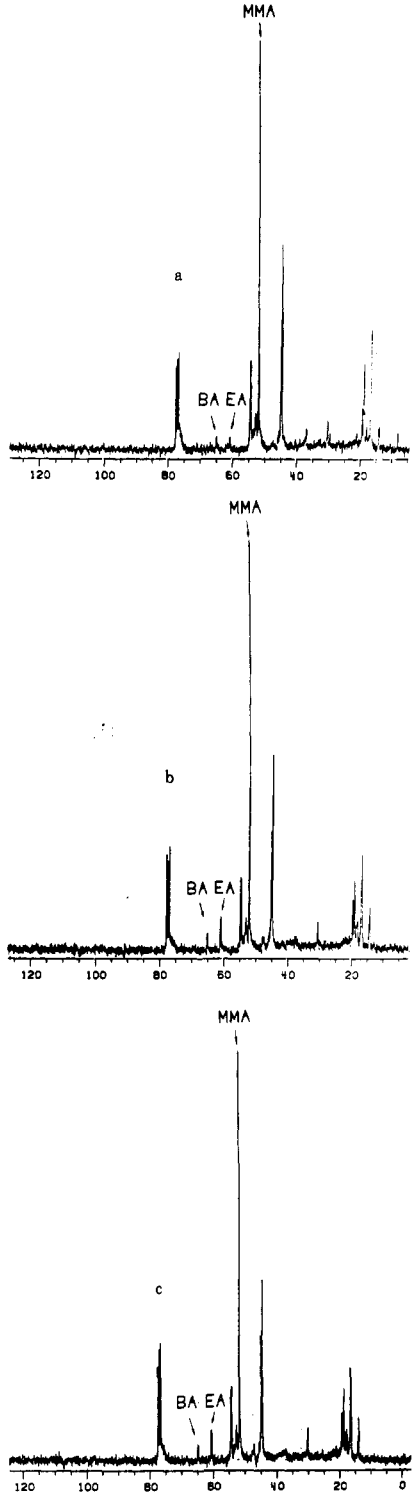

Figure 14. ^{13}C NMR spectra of (a) the high molecular weight fraction of the terpolymer, (b) the unfractionated terpolymer, and (c) the low molecular weight fraction of the terpolymer in deuterated chloroform.

measurements and eq 23 [$a_q^*(K = 0) = H^*C_qM_q\nu_q^2$], which distorts the hydrodynamic size distribution curve on the y axis only because ν_q depends on chain composition. Thus, if we know the relationship between ν_{polym} and chain composition, such as eq 1, we can solve for both the chain composition and the molecular weight distribution.

As the resolution on the characteristic line-width distribution $G(\Gamma)$ is limited, our scheme cannot be used to determine sharp variations in chain composition and/or molecular weight distributions. However, on the basis of the same limitations, if we know k_D and α_D of eq 21 for

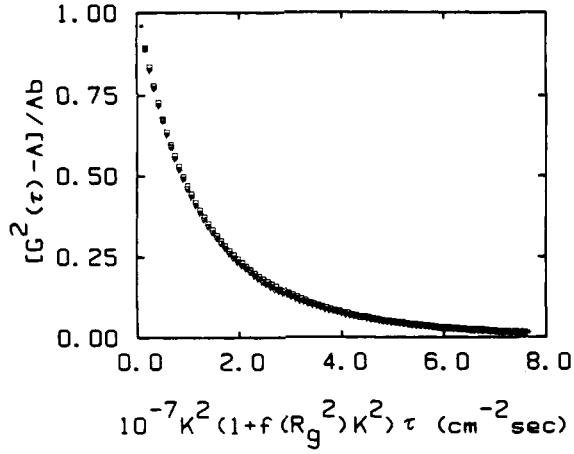

Figure 15. Plot of $[G^{(2)}(\tau) - A]/Ab$ ($\equiv|g^{(1)}(\tau)|^2$) vs. $K^2(1 + f\text{-}\langle R_{g,a}\rangle K^2)$. Hollow squares, $\theta = 45°$; inverted hollow triangles, $\theta = 60°$; stars, $\theta = 90°$. Terpolymer in dioxane at 30 °C. $C = 9.65 \times 10^{-4}$ g/mL.

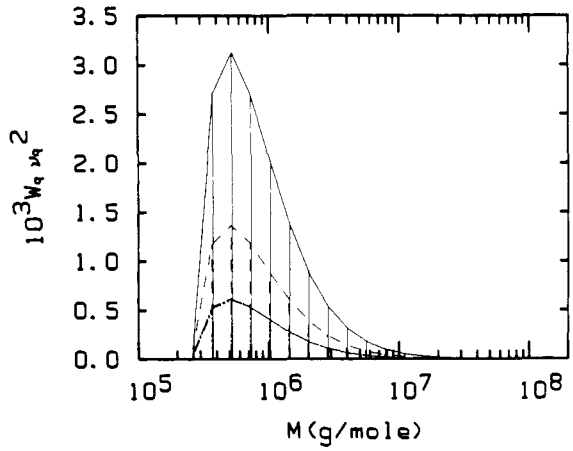

Figure 16. Plot of $W_q\nu_q^2$ vs. M_q at infinite dilution using results of the two solvent pairs MEK–CYC and DIO–CYC: (—) MEK; (- - -) DIO; (-·-, ····) CYC.

two specific solvents, we can determine both the molecular weight distribution and the chain composition without using static light scattering measurements except in the initial calibration.

Acknowledgment. We gratefully acknowledge support of this research project by the U.S. Army Research Office (Contract DAAG29-82K-0143). B.C. thanks W. Shuely, Chemical Research and Development Center, Aberdeen Proving Ground, MD, for helpful comments on solvent selection and information on chain composition by ^{13}C NMR.

Registry No. Acryloid K-125, 25767-43-5; CYC, 108-94-1; MDCB, 541-73-1; MEK, 78-93-3; DIO, 123-91-1; EA, 141-78-6.

References and Notes

(1) Debye, P. *J. Phys. Colloid Chem.* **1947**, *51*, 18.
(2) Bushuk, W.; Benoit, H. *Can. J. Chem.* **1958**, *36*, 1616.
(3) Kambe, H.; Kambe, Y.; Honda, C. *Polymer* **1973**, *14*, 460.
(4) Stockmayer, W. H.; Moore, L. D., Jr.; Fixman, M.; Epstein, B. N. *J. Polym. Sci.* **1955**, *16*, 517.
(5) Leng, M.; Benoit, H. *J. Polym. Sci.* **1962**, *57*, 263.
(6) Prud'homme, J.; Bywater, S. *Macromolecules* **1971**, *4*, 543.
(7) Zilliox, J. G.; Roovers, J. E. L.; Bywater, S. *Macromolecules* **1975**, *8*, 573.
(8) Utiyama, H.; Takenaka, K.; Mizumori, M.; Fukuda, M. *Macromolecules* **1974**, *7*, 28.
(9) Utiyama, H.; Takenaka, K.; Mizumori, M.; Fukuda, M.; Tsunashima, Y.; Kurata, M. *Macromolecules* **1974**, *7*, 515.
(10) Tanaka, T.; Kotaka, T.; Inagaki, H. *Macromoleules* **1974**, *7*, 311; **1976**, *9*, 561.
(11) Tuzar, Z.; Kratohvil, P. *Polym. Lett.* **1969**, *7*, 825.

(12) Kratohvil, P. *J. Polym. Sci., Polym. Symp.* **1975**, *No. 50*, 487.
(13) Huglin, M. B.; Richards, R. W. *Polymer* **1976**, *17*, 588.
(14) Chu, B.; Gulari, Es. *Macromolecules* **1979**, *12*, 445.
(15) DiNapoli, A.; Chu, B.; Cha, C. *Macromolecules* **1982**, *15*, 1174.
(16) Chu, B.; Lee, D.-C. *Macromolecules* **1984**, *17*, 926.
(17) Ford, J. R.; Chu, B. "Proceedings of the 5th International Conference on Photon Correlation Techniques in Fluid Mechanics"; Schulz-Dubois, E. O., Ed.; Springer-Verlag: New York, 1983; pp 303–314.
(18) Stockmayer, W. H.; Schmidt, M. *Pure Appl. Chem.* **1982**, *54*, 407.
(19) Shuely, W., private communication.
(20) See: Huglin, M. B. In "Light Scattering from Polymer Solutions"; Huglin, M. B., Ed.; Academic Press: New York, 1972; p 184.
(21) Koppel, D. E. *J. Chem. Phys.* **1972**, *57*, 4814.
(22) ter Meer, H. U.; Burchard, W.; Wunderlich, W. *Colloid Polym. Sci.* **1980**, *258*, 675.

X-ray Scattering from Polythiophene: Crystallinity and Crystallographic Structure

Z. Mo, K.-B. Lee, Y. B. Moon, M. Kobayashi, A. J. Heeger, and F. Wudl*

Department of Physics, Institute for Polymers and Organic Solids, University of California, Santa Barbara, California 93106. *Received February 13, 1985*

ABSTRACT: X-ray scattering has been used to investigate the crystallinity and crystal structure of chemically coupled polythiophene. Heat treatment at elevated temperatures leads to significant increases in crystallinity (from ~35% as synthesized up to ~56% after annealing at 380 °C for 30 min) and coherence length indicative of chain growth and extension. Chemical analysis of the chain-extended polythiophene shows a major reduction in residual iodine content consistent with growth of the polymer chains to approximately 1200 thiophene rings. An initial model of the crystal structure of polythiophene is presented.

Introduction

Polythiophene (PT) can be viewed as an sp^2p_z carbon chain in a structure (see Figure 1) somewhat analogous to that of *cis*-$(CH)_x$ but stabilized in that structure by the sulfur, which covalently bonds to neighboring carbons to form the heterocycle.[1] Conjugated polymers such as polythiophene are of current interest since they are semiconductors that can be doped, with resulting electronic properties that cover the full range from insulator to metal.[2] Moreover, the polyheterocycles are of specific theoretical interest since the two valence bond configurations sketched in Figure 1b are not energetically equivalent.[3] As a result, the inherent coupling of electronic excitations to chain distortions in such linear conjugated polymers leads to the formation of polarons and bipolarons as the dominant species involved in charge storage and charge transport.

High-quality polythiophene has recently been synthesized by chemical coupling of 2,5-diiodothiophene.[1] On the basis of chemical analysis of the residual iodine content, the chemically prepared polythiophene consists of polymer chains with approximately 45 thiophene rings (~180 carbon atoms along the backbone). This chemically coupled polythiophene contains a relatively small concentration of unpaired spins and a clean IR spectrum, indicative of a stereoregular polymer with a relatively high degree of structural perfection. Moreover, preliminary X-ray scans showed that the polymer is crystalline.[4]

Photoexcitation of neutral PT leads to photogeneration of polarons with associated changes in the visible–IR absorption spectrum and with photoinduced ESR.[5] In situ studies[3] of PT during electrochemical doping have demonstrated that in the dilute regime, charge is stored in bipolarons, weakly confined soliton pairs with a confinement parameter $\gamma \simeq 0.1$–0.2. After doping to saturation with AsF_5 (~24 mol %), the electrical conductivity increases by nearly 10 orders of magnitude[1] to 14 Ω^{-1} cm^{-1}. Moreover, the optical properties,[3] the magnitude and temperature dependence of the thermopower,[1] and the existence of a temperature-independent Pauli spin susceptibility[6] all indicate a truly metallic state for the heavily doped polymer.

Table I
Chemical Composition of Polythiophene (%)

M_r	C	H	S	I	remarks
3958[a]	56.71	2.63	37.05	3.17	as synthesized
	58.67	2.40	39.24	0.13	after annealing at 300 °C
98700	58.43	2.45	38.99	0.13	calcd

[a] 49 ppm Mg and 51 ppm Ni were also present in this sample.

In this paper, we focus on an X-ray scattering investigation of the crystallinity and crystallographic structure of chemically coupled PT. We find that heat treatment at 300 °C for 30 min leads to significant increases in crystallinity (from ~35% as synthesized up to ~52%) and coherence length indicative of chain growth and extension. This is accompanied by loss of iodine; chemical analysis of the chain-extended PT shows a major reduction in residual iodine content consistent with growth of polymer chains to approximately 1200 thiophene rings, or a molecular weight of $\sim 10^5$. From analysis of the powder pattern Bragg diffraction, we have obtained crystallographic data that allow indexing and identification of the unit cell parameters. Based upon one-to-one similarities with the *d* spacings found for poly(*p*-phenylene), an initial model of the structure is presented with two polythiophene chains in the unit cell.

Experimental Techniques

The polythiophene used in these experiments was synthesized by condensation polymerization of 2,5-diiodothiophene as described earlier.[1] The composition (as obtained from chemical analysis) of the as-synthesized polymer is given in Table I. The dark brown powder was packed into an aluminum mold (0.80 in. × 0.40 in × 0.12 in) for heat treatment and subsequent X-ray scattering measurements.

The X-ray scattering apparatus utilizes a Huber 430/440 goniometer, which allows independent horizontal rotations of the sample and the detector with angular resolution of 0.001°. The Cu K_α radiation was provided by a 1-kW Philips X-ray tube (40 kV at 25 mA). As monochromator and analyzer we used flat HOPG crystals. Powder scans were obtained from the as-synthesized polymer and from the same sample after annealing in dry N_2 at 200, 250, 300, and 380 °C for 30 min. In a separate series of experiments, the heat treatment was carried out with the sample in air.

0024-9297/85/2218-1972$01.50/0